Journal of Inclusion Phenomena and Macrocyclic Chemistry (2007) 58:103–114
DOI 10.1007/s10847-006-9129-7

Fluorescence and Molecular Mechanics of 1-Methyl Naphthalenecarboxylate/ Cyclodextrin Complexes in Aqueous Medium

ANTONIO DI MARINO, LAURA RUBIO and FRANCISCO MENDICUTI*
Departamento de Química Física, Universidad de Alcalá, 28871, Alcalá de Henares, Madrid, Spain

(Received: 28 February 2006; in final form: 28 June 2006)

Key words: cyclodextrins, fluorescence, molecular mechanics, 1-methyl naphthalenecarboxylate, 1-methylnaphthoate

Abstract

Steady-state, time-resolved fluorescence and Molecular Mechanics techniques have been used to study the complexation of 1-methyl naphthalenecarboxylate with three naturally occurring cyclodextrins (CDs). Emission spectra of 1MN show two overlapping electronic bands. The stoichiometry, the formation constants of the complexes and the thermodynamics parameters upon inclusion were obtained from the change of intensity ratios R of the maxima of both bands and $\langle\tau\rangle$ with [CD] and temperature. As with the 2-methyl naphthalenecarboxylate (2MN) guest, 1:1 stoichiometries were obtained for all complexes. The formation constants, however, were relatively low compared to those obtained for 2MN. Geometry of the complexes from Molecular Mechanics in the presence of water agrees with the experimental stoichiometry of the complexes and the signs of enthalpy and entropy changes. Quenching, R at [CD] $\rightarrow \infty$ and fluorescence depolarization measurements also support the proposed structures. As with 2MN the inclusion is mostly dominated by van der Waals interactions.

Introduction

Cyclodextrins (CDs) are torus-like macrorings which have a relatively non-polar inner cavity and two hydrophilic rims at both entrances. CDs are capable of forming non-covalent binding inclusion complexes of different stoichiometry and stabilities with low and high molecular weight guests [1–5]. The microviscosity and polarity of the medium surrounding the guest when it penetrates inside the hydrophobic CD cavity change with respect to the free guest in water. This complexation subsequently affects the fluorescence properties of the guest. Stoichiometry, binding constants, thermodynamics parameters accompanying the association and structural information about the geometry of the complexes can be obtained from the change of some fluorescence properties upon complexation. Emission intensity [6–13], excimer formation [14–18], fluorescence depolarization [13, 19–22], the relative intensity of some bands [20, 21, 23–28] and the decay of fluorescence [6, 20, 21, 28–30] are some of these properties. These experimental aspects together with Molecular Modelling [21, 27, 28, 31–33] contribute to clarifying the complexation mechanism and to learning more about the driving forces involved in such processes.

Steady-state fluorescence [34, 35] and Molecular Mechanics calculations [31, 35] were employed to study the complexation of 2-methyl naphthalenecarboxylate (2MN) with the three naturally occurring CDs. More recently additional fluorescence techniques, including time-resolved fluorescence, have also been used [20]. 2MN fluorescence spectra exhibited two electronic emission bands whose intensity ratio R was sensitive to medium polarity. The analysis of the variation of R with [CD] and temperature reveals identical (1:1) stoichiometry for any of the CD complexes at any temperature. The formation constants at 25 °C were similar for 2MN:αCD and 2MN:γCD ($\sim$200 M^{-1}) and ten times larger for 2MN:βCD ($\sim$2000 M^{-1}). Linear van't Hoff plots reveal $\Delta H^0 < 0$, but $|\Delta H^0_{MN:\alpha CD}| > |\Delta H^0_{MN:\beta CD}| > |\Delta H^0_{MN:\gamma CD}|$. ΔS^0 values and signs, however, depend on the CD used, $\Delta S^0_{MN:\beta CD} \approx \Delta S^0_{MN:\gamma CD} > 0$ but $\Delta S^0_{MN:\alpha CD} < 0$. Molecular Mechanics (MM) [31, 35] on 2MN inclusion indicates that 2MN completely penetrates the βCD and γCD cavities, but makes only a slight penetration in the cavity of the αCD. The van der Waals nonbonded host-guest interactions were the main forces of complexation. Both, the most probable structures of the complexes and the type of forces responsible for complexation, account for the values and signs of ΔH^0 and ΔS^0. Fluorescence anisotropy, quenching experiments, average lifetimes $\langle\tau\rangle$ and R_∞ (R at [CD] $\rightarrow \infty$), which is a

* Author for correspondence. E-mail: francisco.mendicuti@uah.es

way to estimate the effective dielectric constant surrounding the guest in the complex, were mostly in agreement with the thermodynamic parameters and the geometry proposed.

In this paper several steady-state and time-resolved fluorescence techniques are employed to study the complexation with α-, β- and γCDs of the 1-methyl naphthalenecarboxylate (1MN), a bulkier 2MN isomer. Stoichiometries, binding constants and the thermodynamics parameters upon complexation were obtained. The combination of fluorescence polarization, quenching, lifetime measurements and the Molecular Mechanics (MM) calculations was used to interpret the changes of enthalpy and entropy upon complexation, which are related to the geometry and the driving forces responsible for the formation of such complexes. Results were compared with those obtained for 2MN.

Materials and methods

Sample preparation

1MN was synthesized and purified as described elsewhere [36]. Karl-Fisher analysis reveals a 9.2%, 11.1% and 10.4% water content by mass for αCD, βCD and γCD respectively (Aldrich). Solvents employed were *n*-alcohols $H(CH_2)_nOH$, from n = 1–7, ethylene glycol (Aldrich spectrophotometric grade or purity > 98%) and deionized water (milli-Q). 1MN/CD water solutions were prepared by weight in their own quartz cells from a 1MN saturated ($\sim 10^{-5}$–10^{-6} M) aqueous solution filtered through cellulose filters (Millipore, 0.45 μm ∅). The content of the cells was stirred for 48 hours before measuring. α-, β- and γCDs concentrations were in the 0–51.8, 0–11.8 and 0–25.4 mM ranges respectively. [1MN] was kept constant in all experiments.

Fluorescence

Steady-state fluorescence and time-resolved measurements were performed by using a SLM 8100 AMINCO and a TCSPC FL900 Edinburgh Instruments spectrofluorimeters. Characteristics and measurement conditions were described previously [21]. The thyratron-gated lamp was filled with hydrogen. Data acquisition was carried out by using 1024 channels with a time window width of 200 ns and a total of 10,000 counts at the maximum. All measurements were performed in the temperature range from 5 to 45 °C at 10 °C intervals (Huber Ministat and Techne TE-8A). Decay intensity profiles were fitted to a sum of exponential decay functions by the iterative reconvolution method [37].

The average lifetime of a multiple-exponential decay function was then defined as

$$\langle \tau \rangle = \frac{\sum_{i=1}^{n} A_i \tau_i^2}{\sum_{i=1}^{n} A_i \tau_i} \tag{1}$$

where A_i is the pre-exponential factor of the component with a lifetime τ_i of the multi-exponential function intensity decay.

The fractional contribution f_i of each decay time to the steady-state intensity at the wavelength of observation, is given by [38]

$$f_i = \frac{A_i \tau_i}{\sum_{i=1} A_i \tau_i} = \frac{I_i}{\sum_{i=1} I_i} \tag{2}$$

On the other hand, the intensity weighted average lifetime $< \tau >$ from a dilute solution of a pair of emitting species, 1 and 2, that do not interact during the excited-state lifetime can be obtained as

$$\langle \tau \rangle = f_1 \tau_1 + f_2 \tau_2 \tag{3}$$

From the fluorescence depolarization measurements, the anisotropy r is defined as [39]:

$$r = (I_{VV} - G I_{VH})/(I_{VV} + 2 G I_{VH}) \tag{4}$$

where I_{xy} is the intensity of the emission that is measured when the excitation polarizer is in position x (V for vertical, H for horizontal), the emission polarizer is in position y, and the G factor ($= I_{HV}/I_{HH}$) corrects for any depolarization produced by the optical system.

For a single excited species which is dynamically quenched with Q, the ratio of fluorescence intensity (area under spectrum), F or lifetime τ in the presence of Q and in its absence ($F_{q=0}$ or $\tau_{q\,=\,0}$) are related to [Q] by the Stern-Volmer equation. The slope of linear Stern-Volmer plots provides the quenching constant K_{SV}, which is also related to a bimolecular quenching constant k_q and lifetime in the absence of quencher $\tau_{q\,=\,0}$. Stern-Volmer $F/F_{q=0}$ vs. [Q] plots are usually non-linear. Curves can be analyzed by using the quenching-sphere-action model [40]. Stern-Volmer equation is then modified as,

$$\frac{F_{q=0}}{F} = \{1 + K_{SV}[Q]\} \exp(vN[Q]/1000) \tag{5}$$

where v (cm^3) is the volume of quencher sphere action, N Avogrado's number and K_{SV} is obtained from linear representations of $\tau/\tau_{q=0}$ (or $<\tau>/<\tau>_{q=0}$) vs. [Q].

For heterogeneous systems like the free and the complexed guest, the quenching parameters can be obtained by modifying the lifetime linear Stern-Volmer equation as

$$\frac{\langle \tau \rangle}{\langle \tau \rangle_{q=0}} = \frac{t_f}{(1 + K_{SV,f}[Q])} + \frac{t_c}{(1 + K_{SV,c}[Q])} \tag{6}$$

and Equation (5) as

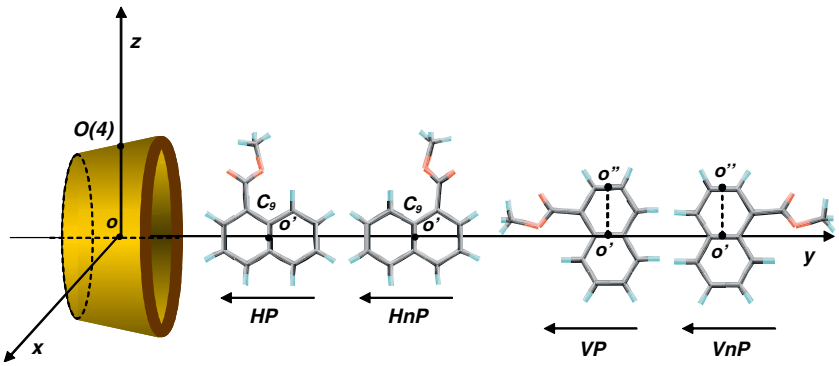

Figure 1. Coordinate systems used to define the 1MN:CD complexation processes. Four orientations *HP, HnP, VP* and *VnP* depicted were considered.

$$\frac{F}{F_{q=0}} = \frac{f_f}{\{1 + K_{SV,f}[Q]\}\exp\left(v_f N[Q]/1000\right)} + \frac{f_c}{\{1 + K_{SV,c}[Q]\}\exp\left(v_c N[Q]/1000\right)} \quad (7)$$

where the t_f and t_c fractions are the contributions to $\langle\tau\rangle_{q=0}$ due to the free and complexed guest in the absence of the quencher; f_f and f_c are the fraction of total fluorescence, already defined, due to both species. If the quencher does not modify the equilibrium for the formation of the complex, f_f , f_c, t_f and t_c are related by:

$$f_f = \frac{\langle\tau\rangle_{q=0} - \tau_{c,q=0}}{\tau_{f,q=0} - \tau_{c,q=0}} \qquad f_c = 1 - f_f$$
$$t_f = \frac{f_f \tau_{f,q=0}}{\langle\tau\rangle_{q=0}} \qquad t_c = 1 - t_f \quad (8)$$

Both equations are derived from Equation (3). $K_{SV,f}$, v_f , $K_{SV,c}$ and v_c are the Stern-Volmer constants and volume of the sphere action for both species.

These parameters were obtained for each system as follows: $K_{SV,f}$ by fitting the time-resolved data of 1MN in the absence of CD to the linear Stern-Volmer equation; $K_{SV,c}$ for each system by adjusting the time-resolved data to Equation (6) by fixing $K_{SV,f}$; the volume v_f from the experimental steady-state data in the absence of CD by fitting them to Equation (5) by fixing $K_{SV,f}$; v_c from the experimental steady-state data in the absence of CD by fitting them to Equation (7) and by fixing other parameters calculated in the previous steps; and $k_{q,f}$ and $k_{q,c}$ from $K_{SV,f}$, $K_{SV,c}$, $\tau_{f,q=0}$ and $\tau_{c,q=0}$.

Molecular mechanics details

MM calculations were performed with Sybyl 6.9 [41] and the Tripos Force Field [42] in the presence of water. Characteristics of these calculations and methods were similar to those described previously [21, 27, 28, 31, 35]. Guest charges were obtained by MOPAC (AM1) [43]. The initial structure of 1MN, depicted in Figure 1, was the most stable after performing a search by changing the torsional angle around the rotational ester bond. For this conformation (one of four local minima) the ester group and the aromatic ring planes angle is 40°. Binding energy, $E_{binding}$ (or any non-bonded energy interaction) between 1MN and CD is obtained as the difference between the potential energy of the system and the sum of the potential energies of the isolated 1MN and CD. Strain energy is the sum of bond stretching, bond angle bending and torsion energy terms. A hydrogen bond is assumed when the O···H–O angle and the O···H distance are in the 120°–180° and 0.8–2.8 Å ranges.

Three parameters (oo' projection on the y coordinate, the angle θ between the yz and the aromatic ring planes and the δ oo'C9 angle) define guest orientation relative to the host. Calculations were performed where 1MN approached the CD by the polar (*P*) or nonpolar (*nP*) sides and by two possible orientations *V* and *H*, as depicted in Figure 1. The most feasible guest-host orientations for the approaching were obtained from the critical analysis of $E_{binding}$, obtained by scanning δ, θ and y parameters in the vacuo. Fixed δ and θ, the 1:1 complexation was simulated by approaching 1MN to the CD along the y coordinate from y = 20 (Å) to −20 (Å) at 0.5 Å steps. Each structure generated was solvated (PBC conditions), optimized and analyzed.

Results and discussion

Absorption and excitation spectra

Absorption spectra for 1MN and 1MN/CD solutions in the 250–350 nm range exhibit a maximum placed at approximately 294 nm and a shoulder at around 320 nm. Absorption increases with the CD content for any of the systems studied. No isoemissive points were observed. Placements of relevant bands observed in the excitation spectra of 1MN nearly match those of the absorption spectra. Spectra in the absence of CD, as well as in presence of it, show a band centered at approximately 305 nm and a shoulder at 320 nm. Spectra intensity decreases and a slight red shift is observed upon increasing [CD].

Emission spectra

Figure 2 depicts the emission spectra for 1MN/CD water solutions upon excitation of 294 nm at 25 °C. Such spectra consist of the overlapping of two bands centered in the 385–390 nm range and at approximately 365 nm. Some characteristics of these spectra are: (a) all systems exhibit isosbestic points which are placed close to the high energy peak, at ~363 nm for 1MN/αCD and 1MN/βCD and at ~355 nm for the system that contains γCD; (b) a quenching of the fluorescence intensity takes place upon addition of CD, the amount of which depends on the type of CD and temperature; the highest intensity variation with [CD] is obtained for the 1MN/γCD system and the lowest for 1MN/αCD; and (c) the spectra do not exhibit any substantial fluorescence shift or broadening

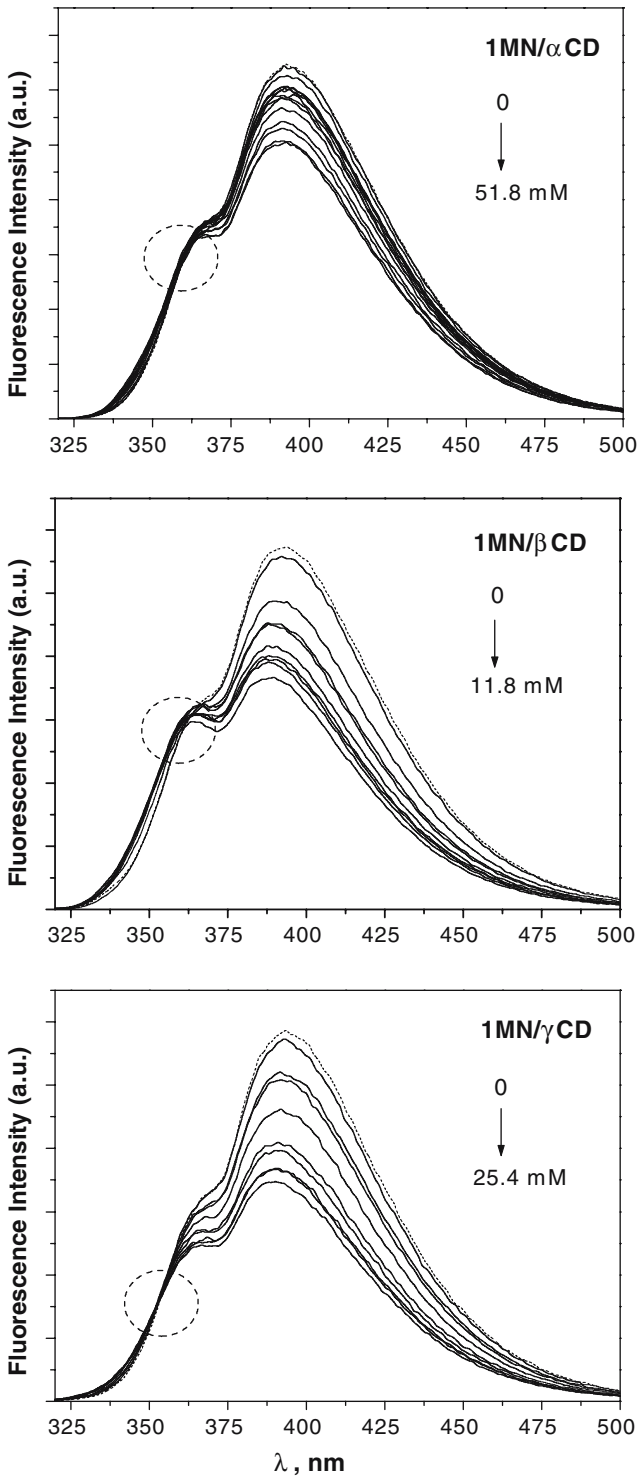

Figure 2. Uncorrected emission spectra of 1MN and 1MN-CD (α-, β- or γCD) aerated aqueous solutions at different [CD] at 25 °C upon λ_{exc} = 294 nm. (top) [αCD] = 0; 0.68; 2.62; 4.60; 6.55; 8.53; 10.47; 12.49; 14.38; 16.36; 22.33; 29.68; 38.26; 44.07 and 51.79 mM. (middle) [βCD] = 0; 0.40; 1.79; 3.17; 4.69; 6.05; 7.50; 8.93; 10.21 and 11.75 mM. (bottom) [γCD] = 0; 0.87; 2.54; 3.98; 6.42; 11.514; 16.61; 18.26; 21.55 and 25.41 mM.

of the monomer emission to the red at any [CD] and temperature that could denote the presence of intermolecular 1MN excimers. The main characteristic, however, is (d) the decreasing experimented by the intensity ratios of the low and high energy bands ($R = I_{\sim 385\,nm}/I_{\sim 365\,nm}$) upon CD addition. The intensity of the low energy band decreases and that of the high one almost remains constant with [CD]. The three left panels in Figure 3 depict the variation of R with [CD] and temperature. These concentrations may even be very close to the αCD solubility limit. The largest variation of R takes place for 1MN/βCD whereas only a small variation occurs for 1MN/αCD. The decreasing in R is associated with the decreasing in polarity of the medium surrounding the guest during complexation. Similar effects were observed with 2MN and other naphthalene derivative guests [11, 13, 20, 21, 27, 28, 34, 35].

Time-resolved fluorescence

Fluorescence intensity decay measurements at 385 nm upon excitation of 294 nm for isolated 1MN and 1MN/CD water solutions were performed in the same temperature range. Intensity profiles of free 1MN can reasonably be fitted to single exponential decay. These single lifetimes, which slightly decrease with temperature from ~7.8 ns at 5 °C to ~7.2 ns at 45 °C, are smaller than those obtained for 2MN (11.5 ns and 10.1 ns at the same temperatures) [20]. Two lifetime components were, however, observed in the presence of CD. One was similar to that of the isolated 1MN and the other one was faster, in the ~7.1–3.2 ns range, and its relative proportion seemed to increase (decrease) with CD (temperature). This component may be ascribed to the complexed form.

The right panels in Figure 3 also depict the variation of $<\tau>$, obtained by Equation (1), with [CD] and temperature for 1MN/CD systems. As with R the largest decrease in $<\tau>$ with [CD] is obtained for 1MN/βCD and the smallest for the 1MN/αCD system. This unusual decrease, only observed by us when 2MN complexed with the modified 2-hydroxypropyl-βCD [20], is a consequence of the larger fraction of the complexed form, which has a faster lifetime component than free 1MN.

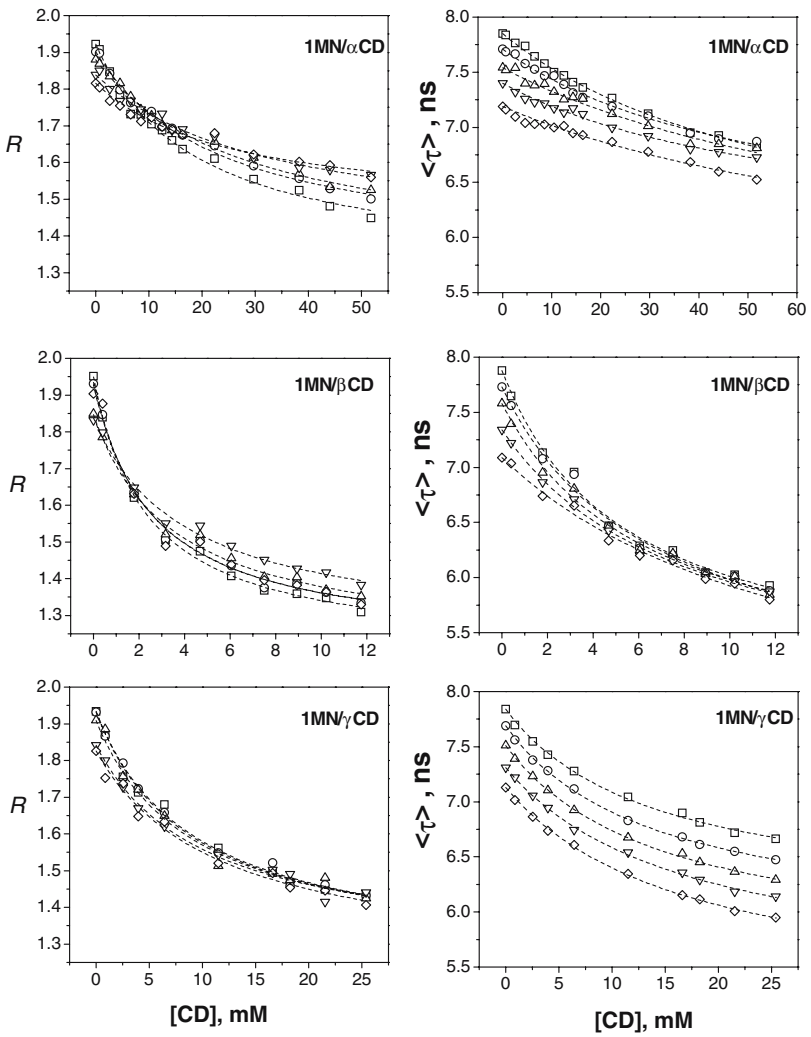

Figure 3. Ratios R of band intensities and average lifetimes $< \tau >$ vs. [CD] at different temperatures, 5 °C (□); 15 °C (○); 25 °C (Δ); 35 °C (∇); and 45 °C (◇). Dashed lines were obtained by adjusting the experimental data to the proper stoichiometry by using Equations (12) and (14).

The physical interpretation of this decreasing will follow in the section Dependence of R_∞ and $<\tau>_\infty$ on medium polarity and microviscosity.

Stability constants and stoichiometry

For a G:CD$_n$ complex, with stoichiometry 1:n, whose global equilibrium can be written as

$$G + nCD \rightleftharpoons G : CD_n \tag{9}$$

the molar fraction of complexed guest (G), x_2 ($\neq f_2$) can be approximated to

$$x_2 = \frac{[G : CD_n]}{[G]_0} = \frac{K\,[CD]_0^n}{1 + K\,[CD]_0^n} \tag{10}$$

where K is the association constant for the equilibrium (9).

On the other hand, the ratio of intensities I_2 and I_1, measured at two emission wavelengths λ_2 and λ_1 respectively, can be defined as

$$R = \frac{I_2}{I_1} = \frac{\phi_{f,2}(1 - x_2) + \phi_{c,2}x_2}{\phi_{f,1}(1 - x_2) + \phi_{c,1}x_2} \tag{11}$$

$\phi_{f,i}$ and $\phi_{c,i}$ are related to the fluorescence quantum yield and molar absorptivities, at the chosen excitation wavelength, for the free and complexed guest respectively.

By substituting x_2 from Equation (10) into Equation (11), R can be related to $[CD]_0$ as follows

$$R = \frac{R_0 + R_\infty(\phi_{c,1}/\phi_{f,1})K[CD]_0^n}{1 + (\phi_{c,1}/\phi_{f,1})K[CD]_0^n} \tag{12}$$

where $\phi_{c,1}/\phi_{f,1} = I_\infty(\lambda_1)/I_0(\lambda_1)$ and R_0 and R_∞ are the values for G and G:CD$_n$ respectively. If the intensity of the guest at λ_1 does not change during complexation $\phi_{c,1}/\phi_{f,1} \approx 1$. Equation (12) can be reorganized as

$$\frac{1}{R - R_0} = \frac{1}{(\phi_{c,1}/\phi_{f,1})K(R_0 - R_\infty)}\frac{1}{[CD]_0^n} + \frac{1}{R_0 - R_\infty} \tag{13}$$

Time-resolved measurements can also provide $<\tau>$. In a similar way, by relating f_f and f_c with x_2 and substituting them into Equation (3) and Equation (10) into the resulting equation, $<\tau>$ can be related to [CD] as,

$$<\tau> = \frac{\tau_0 + \tau_\infty K(\phi_{c,2}/\phi_{f,2})\,[CD]_0^n}{1 + K(\phi_{c,2}/\phi_{f,2})\,[CD]_0^n} \tag{14}$$

by assuming that the lifetime measurements were performed at λ_2 as the emission wavelength. $\phi_{c,2}/\phi_{f,2}$ is related to $\phi_{c,1}/\phi_{f,1}$ as

$$(\phi_{c,1}/\phi_{f,1}) = \frac{R_0}{R_\infty}(\phi_{c,2}/\phi_{f,2}) \tag{15}$$

Equation (15) can be reordered in a linear form like Equations (13).

The following experimental procedure was carried out: (a) $\phi_{c,2}/\phi_{f,2}$ were obtained from the ratio $I_\infty(\lambda_2)/I_0(\lambda_2)$ at each temperature; (b) R_0 were the experimental values of R in the absence of CD and R_∞ were obtained from the steady-state data adjustment to Equation (12) by initially fixing $\phi_{c,1}/\phi_{f,1} = 1$; (c) $\phi_{c,1}/\phi_{f,1}$ were calculated at each temperature by Equation (15) and compared to those obtained directly from $I_\infty(\lambda_1)/I_0(\lambda_1)$; (d) K's were obtained by non-linear Equation (12) from R values with the new $\phi_{c,1}/\phi_{f,1}$ and/or by Equation (14) with the values obtained at step (a) and $<\tau>$ data. They were also obtained by using the linear equations.

Curves depicted in the left and right panels of Figure 3 come from a non-linear regression analysis [44] derived from Equations (12) and (14) respectively. Table 1 collects the association constants obtained from these adjustments and the linear analysis (not depicted) from Equation (13) or similar, as well as, R_∞, τ_∞, $\phi_{c,2}/\phi_{f,2}$ and $\phi_{c,1}/\phi_{f,1}$. Good adjustments indicate stoichiometries 1:1 for all complexes. R_∞ slightly increases with the size of the CD at each temperature. R_0 and τ_0 values (not shown) are quite similar to those for the isolated 1MN at each temperature.

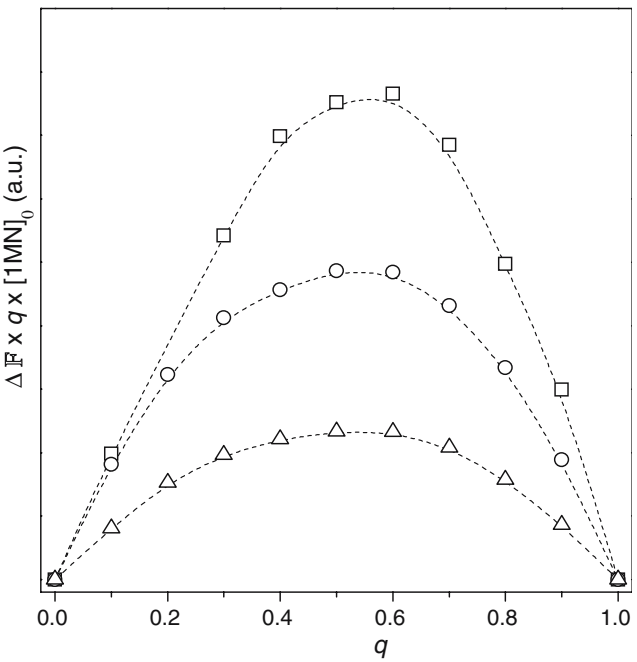

Figure 4. Job's plots for the 1MN/CD systems: αCD (□), βCD (○) and γCD (Δ). $\Delta F = F_0 - F$ is the difference of fluorescence intensity in the absence and in the presence of CD and q is defined as $[CD]_t/([G]_t + [CD]_t)$, where $[CD]_t$ and $[G]_t$ are the CD and G concentrations for each particular measured sample.

Table 1. Equilibrium Constants K, R_∞, τ_∞ $\phi_{c,1}/\phi_{f,1}$ and $\phi_{c,2}/\phi_{f,2}$ parameters obtained from steady-state (ss) and time-resolved (tr) fluorescence measurements at five temperatures for three systems studied

T (°C)	$\phi_{c,1}/\phi_{f,1}$	R_∞	K (M^{-1}) (ss)	$\phi_{c,2}/\phi_{f,2}$	τ_∞	K (M^{-1}) (tr)
1MN/αCD						
5	1.02	1.30 ± 0.03	51 ± 5	0.69	5.60 ± 0.13	24 ± 2
		1.30 ± 0.02	**53 ± 5**		**5.63 ± 0.12**	**24 ± 2**
15	1.04	1.34 ± 0.02	41 ± 3	0.73	5.90 ± 0.14	25 ± 3
		1.35 ± 0.02	**45 ± 3**		**5.94 ± 0.10**	**25 ± 2**
25	1.00	1.33 ± 0.02	35 ± 3	0.71	5.5 ± 0.4	16 ± 4
		1.34 ± 0.02	**36 ± 2**		**6.22 ± 0.10**	**33 ± 4**
35	1.02	1.38 ± 0.03	30 ± 4	0.77	5.91 ± 0.17	21 ± 4
		1.43 ± 0.02	**39 ± 3**		**6.12 ± 0.08**	**28 ± 3**
45	0.95	1.46 ± 0.03	41 ± 6	0.76	5.3 ± 0.4	14 ± 4
		1.48 ± 0.02	**52 ± 6**		**5.7 ± 0.2**	**19 ± 4**
1MN/βCD						
5	0.94	1.20 ± 0.02	454 ± 34	0.58	5.01 ± 0.18	321 ± 47
		1.56 ± 0.01	**447 ± 35**		**5.22 ± 0.07**	**400 ± 28**
15	0.91	1.21 ± 0.03	421 ± 53	0.57	4.8 ± 0.2	263 ± 42
		1.55 ± 0.01	**385 ± 45**		**4.97 ± 0.08**	**301 ± 21**
25	0.94	1.20 ± 0.04	357 ± 72	0.59	4.94 ± 0.17	261 ± 37
		1.54 ± 0.02	**384 ± 63**		**5.19 ± 0.07**	**339 ± 35**
35	0.90	1.21 ± 0.03	320 ± 44	0.59	4.83 ± 0.17	207 ± 27
		1.50 ± 0.01	**309 ± 37**		**4.95 ± 0.06**	**231 ± 17**
45	0.87	1.23 ± 0.03	268 ± 38	0.59	4.3 ± 0.4	123 ± 26
		1.51 ± 0.02	**274 ± 40**		**4.74 ± 0.18**	**165 ± 22**
1MN/γCD						
5	1.11	1.26 ± 0.03	102 ± 12	0.72	6.03 ± 0.07	111 ± 10
		1.60 ± 0.01	**106 ± 12**		**6.05 ± 0.06**	**101 ± 8**
15	1.08	1.25 ± 0.03	99 ± 10	0.70	5.81 ± 0.04	102 ± 5
		1.58 ± 0.01	**133 ± 10**		**5.82 ± 0.05**	**104 ± 6**
25	1.06	1.26 ± 0.04	103 ± 16	0.70	5.59 ± 0.05	96 ± 5
		1.58 ± 0.02	**110 ± 16**		**5.58 ± 0.04**	**97 ± 4**
35	1.00	1.27 ± 0.04	97 ± 15	0.69	5.33 ± 0.07	85 ± 6
		1.53 ± 0.02	**95 ± 12**		**5.35 ± 0.07**	**86 ± 5**
45	1.02	1.23 ± 0.05	85 ± 16	0.69	5.14 ± 0.06	85 ± 5
		1.52 ± 0.03	**97 ± 23**		**5.18 ± 0.06**	**87 ± 5**

K values shown were obtained by adjusting the results to: the non-linear Equations (12) and (14) and (bold) the linear Equations (13).

The association constants obtained from steady-state measurements were relatively low compared to the values for 2MN complexation obtained in a similar way [34, 35]. The average of association constants at 25 °C were ~35, ~385 and ~110 M^{-1} (steady-state) and ~40, ~340 and ~110 M^{-1} (time-resolved) for 1MN complexed with αCD, βCD and γCD respectively. They are smaller than the values for 2MN. The values of $\phi_{c,1}/\phi_{f,1}$ are close to 1 (at λ_{em} = 365 nm $\phi_{c,1} \approx \phi_{f,1}$) and they seem to slightly decrease with temperature. Values of $\phi_{c,2}/\phi_{f,2}$ stay around 0.6–0.7 (at λ_{em} = 385 nm $\phi_{c,2} < \phi_{f,2}$). They do not show any apparent trend with temperature.

The Job's Plots [45, 46] depicted in Figure 4 correspond to a 1:1 stoichiometry for all the 1MN/CD complexes studied.

Enthalpy and entropy changes

ΔH^0 and ΔS^0 from Table 2 were obtained from linear van't Hoff plots depicted in Figure 5 by using the average of K's collected in Table 1. Table 2 also shows ΔH^0 and

Table 2. Values of the enthalpy (ΔH^0) and entropy (ΔS^0) changes during the complexation processes of 1MN with α-, β- and γCD from the average of the values of K obtained by steady-state (ss) and time-resolved (tr) fluorescence measurements

Host	ΔH^0_{ss} (kJ mol^{-1})	ΔS^0_{ss} (JK^{-1} mol^{-1})	ΔH^0_{tr} (kJ mol^{-1})	ΔS^0_{tr} (JK^{-1} mol^{-1})
αCD	−15 ± 7 (−31 ± 1)	−21 ± 25 (−60 ± 2)	+3.3 ± 0.4	+38.2 ± 1.3
βCD	−18 ± 3 (−15 ± 2)	−15 ± 11 (+12 ± 5)	−13 ± 4	+1 ± 14
γCD	−3 ± 2 (−10 ± 3)	+25 ± 7 (+11 ± 8)	−4.8 ± 1.3	+22 ± 4

In parentheses are the values for 2MN taken from references 34 and 35.

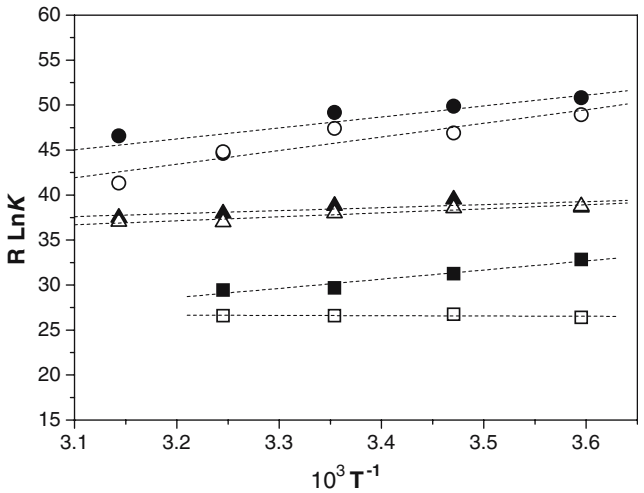

Figure 5. Van't Hoff plots of RLn K vs. T^{-1} for the formation of 1MN complexes with αCD (□), βCD (○) and γCD (Δ) from the average of association constants obtained by steady-state (open symbols) and lifetime (solid symbols) measurements. Values at 45° for 1MN/αCD were discharged due to the large uncertainties.

ΔS^0 for 2MN:CD complexes obtained from steady-state measurements [34, 35]. All systems, except the 1MN/αCD one, present values of thermodynamics parameters obtained from steady-state and time-resolved (less reliable due to intrinsic reasons) methods which are within the standard deviation. ΔH^0 for the formation of 1MN:CD are negative which is typical of large guests trying to penetrate into a relatively small cavity, but quantitatively seem to be slightly smaller than the ones obtained for 2MN:CD [34, 35]. Negative enthalpy changes during complexation are generally attributed to attractive van der Waals and/or hydrogen bonding interactions. A decrease in these interactions usually means a decrease in the absolute ΔH^0 values, as occurs for the 2MN inclusion when the CD size increases [34, 35] or when using 2-hydroxypropyl substituted CDs instead of naturally unsubstituted ones [13]. The entropy changes reveal negative values for 1MN:αCD and 1MN:βCD, which are accompanied by large uncertainties, as well as, positive ones for 1MN:γCD. In fact, in the later case, the process is entropically governed. $\Delta S^0 < 0$ are also characteristic of bulky guests whose penetration into the relatively small cavity is rather limited and/or its movement is also fairly hindered due to large host-guest interactions. The $\Delta S^0 > 0$ for 1MN:γCD, as for 2MN:γCD, may indicate that the 1MN penetration into the γCD cavity is feasible. The location of the ester group may obviously have to do with the differences in ΔH^0 and ΔS^0 for 1MN and 2MN.

Fluorescence depolarization

The fluorescence anisotropy, r, was obtained by using Equation (4) at different temperatures (λ_{ex} = 294 nm; λ_{em} = 385 nm). The upper panel in Figure 6 depicts the change of r with [CD] and temperature for the 1MN/αCD system. The variation with [CD] at each temperature was fitted to an equation similar to Equations (12) or (14), under the assumption that the total anisotropy is the sum of the contribution due to the free and complexed guest. As Figure 6 shows, r increases with [CD] and it decreases with temperature. This can be attributed to the larger fraction of the 1MN complexed and to the viscosity solvent decrease and/or to the presumably decreases in the complexed fraction (if $\Delta H^0 < 0$). r extrapolated at [CD] $\rightarrow \infty$ varies as $r_{\infty,1MN:\gamma CD} > r_{\infty,1MN:\alpha CD} > r_{\infty,1MN:\beta CD} > > r_{0,1MN}$. This variation is obviously related to the size and structure of the complex, the intermolecular 1MN-CD interactions and the movement of the guest inside the cavity. A similar trend was observed for 2MN/CD systems [35].

Dependence of R_∞ and $<\tau>_\infty$ on medium polarity and microviscosity

R_∞ and $<\tau>_\infty$ can also supply additional information about the polarity and microviscosity of the medium surrounding 1MN, as well as, on the location of the guest when complexed. Emission spectra and lifetime measurements for 1MN in different solvents covering a wide polarity (ϵ) and viscosity (η) range were performed at 25°C. The dependence of R with ϵ at 25 °C, which is

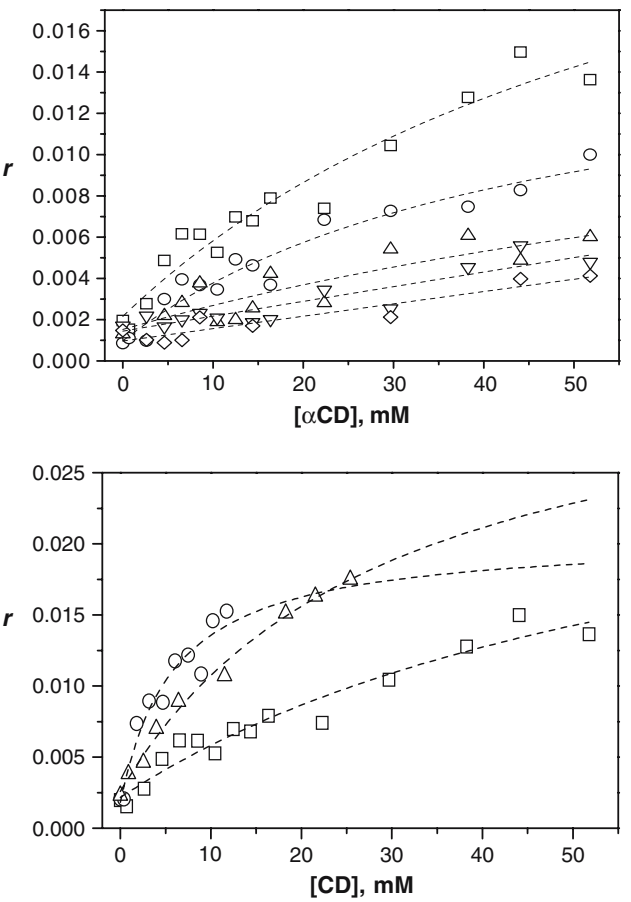

Figure 6. (top) Anisotropies, r, changes with [αCD] and temperature for the 1MN/αCD system; T = 5 °C (□); 15 °C (○); 25 °C (Δ); 35 °C (∇); and 45 °C (◇). (bottom) Variation of r with [CD] for 1MN/CD systems at 5 °C: αCD ((□), βCD (○) and γCD (Δ).

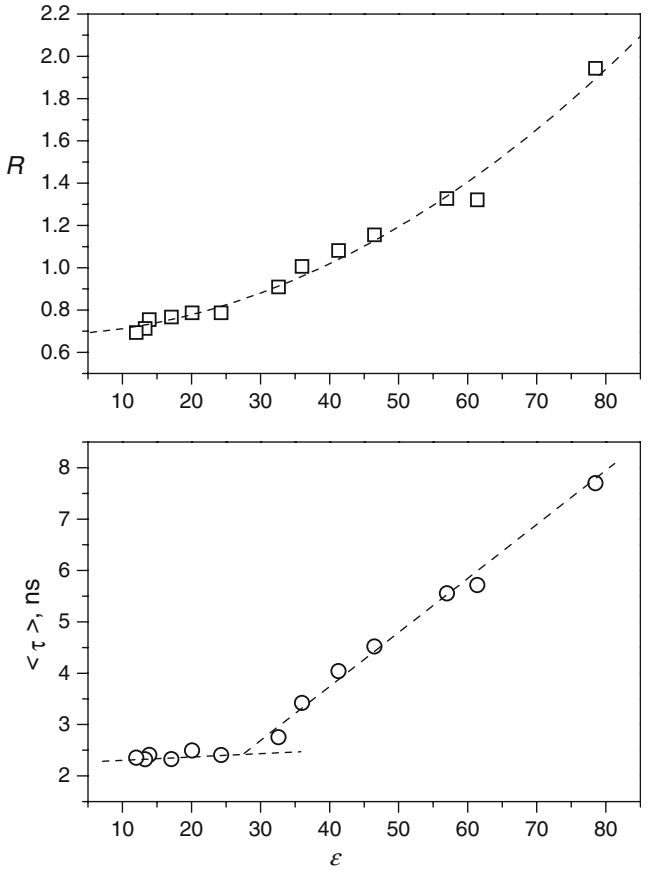

Figure 7. Plots of R and $< \tau >$ vs. the solvent dielectric constant, ϵ for dilute solutions of 1MN in different solvents at 25 °C. Solvents are methanol/water (MeOH:W) and ethanol/water (EtOH:W) mixtures (% volume), and a series of *n*-alcohols (MeOH, EtOH, PrOH, BuOH, PeOH, HeOH and HpOH).

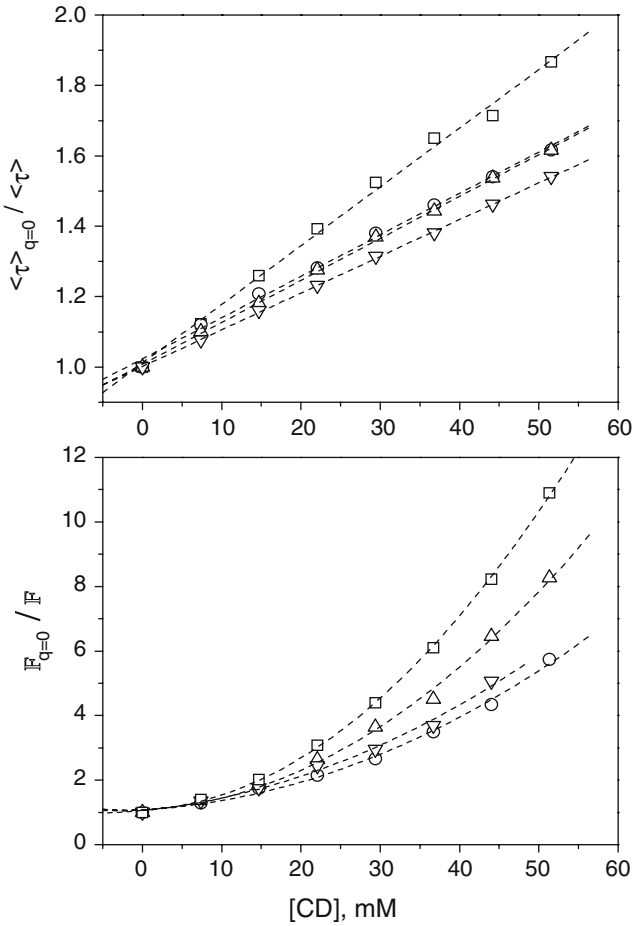

Figure 8. Stern-Volmer representations obtained from time-resolved (top) and steady-state (bottom) measurements at 25 °C for free 1MN (□), 1MN/αCD (○), 1MN/βCD (Δ) and 1MN/γCD (▽). Quencher was 2,3-butanedione (diacetyl).

depicted in Figure 7, was described by $R = 0.68 + 1.1\times10^{-3}\ \epsilon + 1.8\times10^{-4}\ \epsilon^2$. The continuousness of the curve and the relatively wide range of solvent viscosities covered, infers that R depends almost exclusively on polarity. The average of R_∞ from the data collected in Table 1 at 25 °C allows us to estimate ϵ values of 57 ± 1, 59 ± 8 and 61 ± 7 for 1MN complexes with α-, β- and γCDs. 1MN when complexed with any of the CDs is placed in an analogous polarity microenvironment. These values contrast with those of ∼10, ∼49 and ∼74 obtained for 2MN with the same CDs, which are in agreement with the values for the inner α-, β- and γCD cavities estimated by us [27, 34, 35] and other authors [47, 48] using other fluorescence probes. MM calculations and experiments revealed that 2MN can penetrate into the three CDs cavities, even if partially within αCD [31, 34, 35].

Decay profiles of 1MN dilute solutions of organic solvents show a behavior different than that obtained for 1MN in water. When 1MN is measured in methanol/water and ethanol/water mixtures two lifetime components of ∼2.0 ns and ∼8.0 ns are obtained, increasing the contribution of the large one with the water content. Decays of 1MN in other alcohols are also two-exponential. This unexpected heterogeneity differs from that of 2MN whose decay profiles were fitted to a single exponential in the same solvents [20]. It could be related to the different heights of the rotational barriers around the C^{ar}–CO ester bond in both 1MN and 2MN compounds, which are considerably smaller for 1MN than for 2MN [36, 49].

$< \tau >$ depicted at the bottom of Figure 7 as a function of ϵ shows two different behaviors. For solvents with $\epsilon > 30$, $< \tau >$ increases with the polarity and a certain independence of viscosity is observed; and with $\epsilon < 30$, $< \tau >$ is almost constant, probably because of the balance of both polarity and viscosity effects. This also contrasts with the results for 2MN, where $< \tau >$ strongly increases with solvent viscosity for approximately $\epsilon < 30$ [20]. Values of τ_∞ collected in Table 1, which are in the 5–6 ns range at 25 °C, permit us to estimate ϵ values around 55–60 for the medium surrounding 1MN in the complexes. These values are comparable to the ones predicted from R_∞.

The results also explain the monotonic decrease in R and $< \tau >$ with [CD]. This may be due to the decrease in the medium polarity surrounding 1MN when it migrates from an aqueous medium (ϵ∼78) to one of $\epsilon \approx$ 55–60.

Table 3. Parameters of the modified Stern-Volmer equation for quenching of free 1MN and 1MN/CD complexes at 25 °C

System	$\tau_{c,q=0}$ ($\tau_{f,q=0}$) (ns)	$<\tau>_{q=0}$ (ns)	f_f	t_f	$K_{SV,c}$ ($K_{SV,f}$) (M^{-1})	$k_{q,c}\times10^{-9}$ ($k_{q,f}\times10^{-9}$) ($M^{-1}\,s^{-1}$)	$v_c\times10^{-3}$ ($v_f\times10^{-3}$)($Å^3$)
1MN	(7.6 ± 0.1)	7.6	–	–	(16.8 ± 0.4)	(2.22 ± 0.06)	(57.9 ± 0.4)
1MN/αCD	5.5 ± 0.4	6.5	0.48	0.56	8.20 ± 0.50	1.50 ± 0.20	29.9 ± 1.1
1MN/βCD	4.9 ± 0.2	5.9	0.38	0.48	8.73 ± 0.14	1.78 ± 0.09	52.7 ± 1.0
1MN/γCD	5.6 ± 0.1	6.2	0.33	0.40	7.19 ± 0.08	1.29 ± 0.02	44.1 ± 1.1

Quencher was diacetyl, $x_2 = 0.75$ and $\lambda_{ex} = 294$ nm.

Quenching measurements

Figure 8 depicts Stern-Volmer plots from time-resolved (upper panel) and steady-state (lower panel) quenching measurements at 25 °C. They were carried out in free 1MN and 1MN/CD solutions (at $x_2 = 0.75$) by using diacetyl $(CH_3CO)_2$. The value of R does not change upon quencher addition for any of the systems studied. $\langle\tau\rangle_{q=0}/\langle\tau\rangle$ varies linearly with [Q] showing the largest slope for free 1MN. However, $F_{q=0}/F$ plots deviate from the linearity and the largest deviation is observed for 1MN in the absence of CD. Parameters collected in Table 3 were obtained by fitting the experimental data to the quencher sphere of action model for heterogeneous systems with the procedure described before. The following considerations are derived: (a) f_f ranges from 0.33 to 0.48 which means that when $x_2 = 0.75$, the contribution to the total fluorescence intensity is slightly larger for the complexed form, despite the fact that the fluorescence quantum yield of complexed 1MN is always smaller than for free 1MN. The value of t_f varies from 0.40 to 0.56. $K_{SV,c}$ for the complexes are smaller by a factor of two than the $K_{SV,f}$, following $K_{SV,1MN} > K_{SV,1MN:\beta CD} > K_{SV,1MN:\alpha CD} > K_{SV,1MN:\gamma CD}$.

An analogous trend can be inferred for $k_{q,c}$. These results agree that access of quencher to the free 1MN is easier than to the complexed one, but also that the accessibility to 1MN is only slightly larger for 1MN:βCD and 1MN:αCD than for 1MN:γCD. Something similar occurred when comparing free and complexed 2MN. Nevertheless, here the largest quencher- to-guest accessibility is for 2MN:αCD, followed by 2MN:γCD and then 2MN:βCD [35].

Molecular mechanics

Figure 9 depicts changes of $E_{binding}$, van der Waals and electrostatic contributions for 1MN approaching α-, β- and γCDs for the orientations that provide the most favorable interaction energies. Nevertheless, for the 1MN/αCD system the results for two different orientations, which provide similar changes of $E_{binding}$, are shown. Other orientations are less favorable. 1MN/αCD system exhibit a very high repulsive barrier around $y = 0$. This is, however, considerably smaller for 1MN/βCD and it hardly appears for 1MN/γCD. Responsible for these barriers are the repulsive strong ester group-CD (naphthalene-CD) interactions for HP and HnP (for VP and

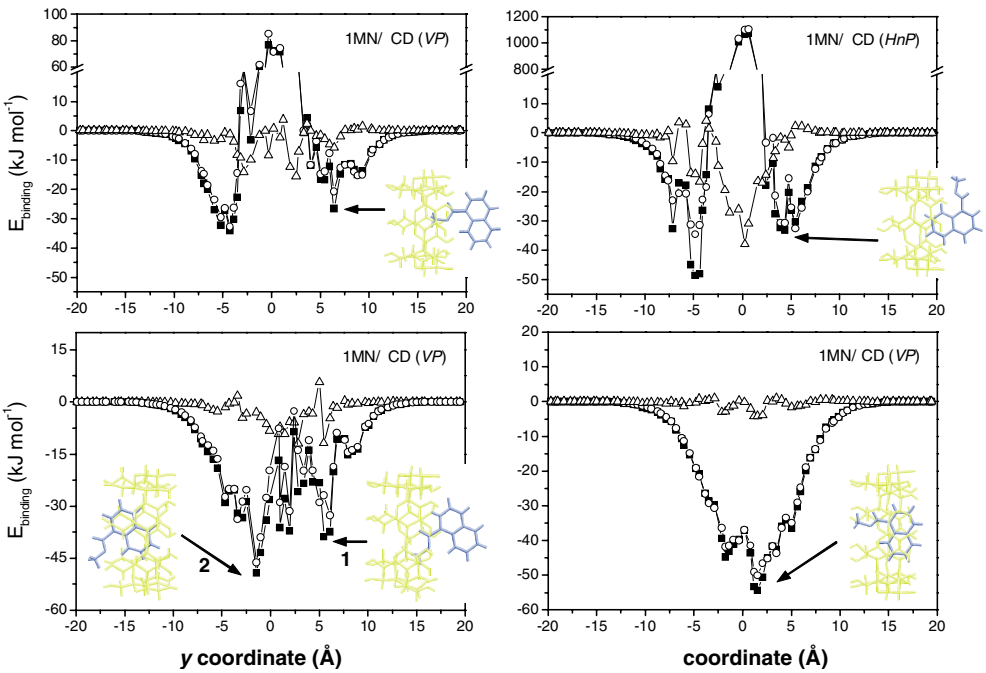

Figure 9. Van der Waals (○) and electrostatic (Δ) contributions to $E_{binding}$ (■) as a function of y coordinate (Å) for 1MN:CD complexation processes. Superimposed are the structures (water removed) of minimum binding energy (MBE).

VnP) orientations. This indicates that 1MN could penetrate into the γCD cavity and a small barrier must be surmounted to enter into βCD. However, 1MN may have no chance at all, whatever its orientation is, to access the αCD cavity. Figure 9 also shows superimposed the structures of minima binding energies (MBE). These are reached at $y = 4.4$ Å; $E_{MBE} = -33.1$ kJ mol^{-1} ($y = 6.4$ Å; $E_{MBE} = -26.5$ kJ mol^{-1}) for the *HnP* (*VP*) orientation of 1MN/αCD. When 1MN approaches βCD, assuming that the small barrier is surmounted, the structure of MBE is achieved for $y = -1.5$ Å ($E_{MBE} = -49.4$ kJ mol^{-1}) if not $y = 5.5$ Å ($E_{MBE} = -38.9$ kJ mol^{-1}). The MBE structure for 1MN/γCD is reached at $y = -1.5$ Å ($E_{MBE} = -54.3$ kJ mol^{-1}). The 1MN guest penetrates totally into the γCD but only a small portion enters the αCD. At a point between is the 1MN:βCD complex. The guest could either enter the cavity (2) or most of it may remain outside (1) if the barrier is not surmounted while approaching. The structure (1) will allow for the formation of intermolecular hydrogen bonds between CD (secondary OH) and 1MN (carboxylic oxygen). In a similar way the *VP* structure for the 1MN:αCD complex can also form intermolecular 1MN-CD hydrogen bonds.

The fact that most of the guest molecule is shielded by the γCD and only little is by αCD could confirm that the breaking of the ordered water around the guest and inside the host cavity upon complexation is mainly be responsible for the ΔS^0 sign during complexation, as they increase and decrease respectively. Nevertheless, the loss of freedom degrees may contribute to the $\Delta S^0 < 0$ for the 1MN/αCD system more than for the 1MN/γCD one. These structures may corroborate the similarity in r_∞ for both complexes. The rotational diffusion rates are very similar due to the comparable structure size for both complexes and/or the fact that the 1MN movement in the complex would be more hindered in the complex with the smallest αCD than in that with the γCD one. These structures would also agree with the differences in $k_{q,c}$ and other quenching parameters for both systems. R_∞ should agree with the fact that 1MN is not totally located inside the αCD cavity, as this cavity is rather more hydrophobic. Similar results were obtained for 2MN:αCD and 2MN:γCD complexes [31, 35].

The 1MN:βCD complex shows $\Delta S^0 < 0$, which could be very close to zero if we take the uncertainties in the experiments into account. A hypothetical $\Delta S^0 > 0$ may agree with a structure where 1MN penetrates almost totally into the cavity, as occurred with 2MN [35], and a $\Delta S^0 < 0$ with an incomplete penetration. In fact, the relatively high value for $k_{q,c}$ would correspond to a partial penetration. The polarity surrounding 1MN seems to be slightly higher than the one proposed for the inner βCD which may also be indicative of a partial penetration. However, the low r_∞ compared to the values for other 1MN:αCD and 1MN:γCD complexes, may point toward a high rotational diffusion rate, which usually means a deep penetration into the cavity. Perhaps both (1) and (2) structures are feasible.

Most of the $E_{binding}$ at the MBE is due to non-bonded van der Waals interactions. Electrostatics, mainly due to ester group-CD interactions, only represents 6–30% of the total binding energy. This contribution increases as the CD size decreases and it hardly appears in γCD complexes. The amount of this contribution, which is mostly favored for *V* orientations, has to do with the location of the ester group close to the secondary CD rim. Complexation generally causes a slight decrease in the total potential energy for 1MN/CD systems. Mainly responsible for such decreases are the non-bonded van der Waals interactions, although they are not the largest contributions to the total energy. The electrostatics interactions hardly change upon complexation. The strain energy, correlated to the relative cavity-guest sizes, is the main contribution to total energy and it slightly increases when 1MN approaches the α- and βCDs and decreases when it approaches the wider γCD cavity.

Conclusions

The 1MN guest forms complexes with α-, β- and γCDs with stoichiometries 1:1, but their stability constants are smaller than for those with the less bulkier 2MN isomer. Molecular Mechanics proves the viability of such complexes. The non-bonded van der Waals interactions are mainly responsible for the stability of the complexes. The formation of complexes is accompanied by negative enthalpy changes that are also smaller than those obtained for 2MN. These negative enthalpies agree with the fact that the van der Waals attractive CD-guest interactions are mainly responsible for the complexation. Entropy changes during complexation may mainly be attributed to the loss of the ordered water around the guest and host cavity upon complexation.

Acknowledgements

This research was supported by Comunidad de Madrid (CAM projects: GR/MAT/0810/2004; S-055/MAT/0227), CICYT (project CTQ2005-04710/BQU) and Universidad de Alcalá (grant to A.D.M.). We wish to express our thanks to M.L. Heijnen for assistance with the preparation of the manuscript.

References

1. J. Szejtli and T. Osa: *Comprehensive Supramolecular Chemistry: Cyclodextrins*, Elsevier, Oxford (1996).
2. V.T. D'Souza and K.B. Lipkowitz: *Chem. Rev.* **98**, 1741 (1998).
3. A. Harada: *Adv. Polym Sci.* **133**, 141 (1997).
4. A. Nepogodiev and J.F. Stoddart: *Chem. Rev.* **98**, 1777 (1998).
5. A. Harada: *Acc. Chem. Res.* **34**, 456 (2001).
6. L. Flamigni: *J. Phys. Chem.* **97**, 9566 (1993).
7. S. Monti, G. Köhler, and G. Grabner: *J. Phys. Chem.* **97**, 13011 (1993).

8. J.M. Schuette and I.M. Warner: *Talanta* **41**, 647 (1994).
9. E.K. Fraiji, T.R. Cregan, and T.C. Werner: *Appl. Spectrosc.* **48**, 79 (1994).
10. A. Nakamura, S. Sato, K. Hamasaki, A. Ueno, and F. Toda: *J. Phys. Chem.* **99**, 10952 (1995).
11. J.M. Madrid, M. Villafruela, R. Serrano, and F. Mendicuti: *J. Phys. Chem B.* **103**, 4847 (1999).
12. M. Shannigrahi and S. Bagchi: *Chem. Phys. Lett.* **403**, 55 (2005).
13. A. Di Marino and F. Mendicuti: *Appl. Spectrosc.* **58**, 823 (2004).
14. N.J. Turro, T. Okubo, and G.C. Weed: *Photochem. Photobiol.* **35**, 325 (1982).
15. K. Kano, I. Takenoshita, and T. Ogawa: *Chem. Lett. Chem. Soc. Jpn.* 231 (1982) .
16. S. Hamai: *Bull. Chem. Soc. Jpn.* **55**, 2721 (1982).
17. S. Hamai: *J. Phys. Chem.* **93**, 6527 (1989).
18. G. Pistolis: *Chem. Phys. Lett.* **304**, 371 (1999).
19. G.C. Catena and F.V. Bright: *Anal. Chem.* **61**, 905 (1989).
20. A. Di Marino and F. Mendicuti: *Appl. Spectrosc.* **56**, 1579 (2002).
21. I. Pastor, A. Di Marino, and F. Mendicuti: *J. Phys. Chem. B* **106**, 1995 (2002).
22. Y. Xu and M.E. McCarrol: *J. Phys. Chem. B* **109**, 8144 (2005).
23. K.W. Street and W.E. Acree: *Appl. Spectrosc.* **43**, 1315 (1988).
24. A. de Muñoz la Peña, T.T. Ndou, J.B. Zung, and I.M. Warner: *J. Phys. Chem.* **95**, 3330 (1991).
25. A. de Muñoz la Peña, T.T. Ndou, J.B. Zung, K.L. Greene, D.H. Live, and I.M. Warner: *J. Phys. Chem.* **113**, 1572 (1991).
26. A.Y. Will, A. de Muñoz la Peña, T.T. Ndou, and I.M. Warner: *Appl. Spectrosc.* **47**, 277 (1993).
27. M. Cervero, A. Di Marino, and F. Mendicuti: *J. Phys. Chem. B* **104**, 1572 (2000).
28. I. Pastor, A. Di Marino, and F. Mendicuti: *J. Photochem. Photobiol.* **173**, 238 (2005).
29. G. Nelson, G. Patonay, and I.M. Warner: *Appl. Spectrosc.* **41**, 1235 (1987).
30. T. Yorozu, M. Hoshino, and M. Imamura: *J. Phys. Chem.* **86**, 4426 (1982).
31. J.M. Madrid, J. Pozuelo, F. Mendicuti, and W.L. Mattice: *J. Colloid Interface Sci.* **193**, 112 (1997).
32. M.J. Sherrod: In J.E.D. Davies (ed.), *Spectroscopic and Computational Studies of Supramolecular Systems*, Kluwer, Dordrecht, The Netherlands (1985) p. 187.
33. E. Cervelló, F. Mazzucchi, and C. Jaime: *J. Mol. Struct. (Theochem)* **530**, 155 (2000).
34. J.M. Madrid and F. Mendicuti: *Appl. Spectrosc.* **51**, 1621 (1997).
35. J.M. Madrid, F. Mendicuti, and W.L. Mattice: *J. Phys. Chem B.* **102**, 2037 (1998).
36. F. Mendicuti, B. Patel, and W.L. Mattice: *Polymer* **31**, 1877 (1990).
37. D.V. ÓConnor, W.R. Ware, and J.C. André: *J. Phys. Chem.* **83**, 1333 (1979).
38. J.R. Lakowicz: *Principles of Fluorescence Spectroscopy*, 2nd ed., Kluwer, New York (1999), pp. 129.
39. J.R. Lakowicz: *Principles of Fluorescence Spectroscopy*, 2nd ed., Kluwer, New York (1999), pp. 298.
40. B. Valeur: *Molecular Fluorescence: Principles, Applications*, Wiley-VCH, Weinheim (2002), pp. 89.
41. Sybyl 6.9. Tripos associates, St. Louis, Missouri, USA.
42. M. Crark, R.C. Cramer III, and N. van Opdenbosch: *J. Comput. Chem.* **10**, 982 (1989).
43. MOPAC (AM1), included in the Sybyl package.
44. MicroCal Origin 6.0, MicroCal Software, Inc. Northampton, MA, USA.
45. P. Job: *Ann. Chim.* **9**, 113 (1928).
46. Y.L. Loukas: *J. Phys. Chem. B* **101**, 4843 (1997).
47. K.W. Street Jr. and W.E. Acree Jr.: *Appl. Spectrosc.* **43**, 1315 (1988).
48. B.D. Wagner and P.J. MacDonald: *J. Photochem. Photobiol.A.* **114**, 151 (1998).
49. O. Martín: PhD Thesis, Universidad de Alcalá, Alcalá de Henares, Madrid (1998).